

# Liquid flooded flow-focusing microfluidic device for in situ generation of monodisperse microbubbles

Ali H. Dhanaliwala · Johnny L. Chen ·  
Shiyang Wang · John A. Hossack

Received: 24 June 2012 / Accepted: 7 September 2012 / Published online: 6 October 2012  
© Springer-Verlag Berlin Heidelberg 2012

**Abstract** Current microbubble-based ultrasound contrast agents are administered intravenously resulting in large losses of contrast agent, systemic distribution, and strict requirements for microbubble longevity and diameter size. Instead we propose in situ production of microbubbles directly within the vasculature to avoid these limitations. Flow-focusing microfluidic devices (FFMDs) are a promising technology for enabling in situ production as they can produce microbubbles with precisely controlled diameters in real-time. While the microfluidic chips are small, the addition of inlets and interconnects to supply the gas and liquid phase greatly increases the footprint of these devices preventing the miniaturization of FFMDs to sizes compatible with medium and small vessels. To overcome this challenge, we introduce a new method for supplying the liquid (shell) phase to a FFMD that eliminates bulky interconnects. A pressurized liquid-filled chamber is coupled to the liquid inlets of an FFMD, which we term a flooded FFMD. The microbubble diameter and production rate of flooded FFMDs were measured optically over a range of gas pressures and liquid flow rates. The smallest FFMD manufactured measured  $14.5 \times 2.8 \times 2.3$  mm. A minimum microbubble diameter of  $8.1 \pm 0.3$   $\mu\text{m}$  was achieved at a production rate of 450,000 microbubbles/s (MB/s). This represents a significant improvement with respect to any previously reported result. The flooded design also simplifies parallelization and production rates of up to 670,000 MB/s were achieved using a parallelized version of the flooded FFMD. In addition, an intravascular ultrasound (IVUS) catheter was coupled to the flooded

FFMD to produce an integrated ultrasound contrast imaging device. B-mode and IVUS images of microbubbles produced from a flooded FFMD in a gelatin phantom vessel were acquired to demonstrate the potential of in situ microbubble production and real-time imaging. Microbubble production rates of 222,000 MB/s from a flooded FFMD within the vessel lumen provided a 23 dB increase in B-mode contrast. Overall, the flooded design is a critical contribution towards the long-term goal of utilizing in situ produced microbubbles for contrast enhanced ultrasound imaging of, and drug delivery to, the vasculature.

**Keywords** Microfluidics · Flow-focusing · Monodisperse microbubbles · Flooded input · In situ production

## 1 Introduction

Microbubbles, comprising shell stabilized gas bubbles, are ideal ultrasound contrast agents as their high compressibility and low density make them highly echogenic. As a result, microbubbles have been developed to enable or to enhance a wide range of ultrasound applications including: detection of cardiac wall motion abnormalities (Chahal and Senior 2010; Mulvagh et al. 2000), molecularly targeted imaging (Dayton and Rychak 2007; Gessner and Dayton 2010), targeted drug delivery (Böhmer et al. 2009; Ferrara et al. 2007), blood perfusion measurements (Wei et al. 1998), and tumor coagulation therapy (Meloni et al. 2006).

The most common method for microbubble production is agitation (Fritz et al. 1997; Keller et al. 1987; Klibanov 2002), in which a low solubility gas is dispersed within a liquid solution containing a stabilizing shell material. Agitation methods can produce large quantities of microbubbles ( $>10^9$  microbubbles/batch); however, these populations

A. H. Dhanaliwala · J. L. Chen · S. Wang · J. A. Hossack (✉)  
Department of Biomedical Engineering, University of Virginia,  
Charlottesville, VA 22903, USA  
e-mail: jh7fj@virginia.edu

usually have a large size distribution and can have a polydispersity index (i.e.  $SD/mean$ ) (Farook et al. 2009) as high as 150 % (Stride and Edirisinghe 2009). Polydisperse populations of microbubbles have also been shown to have a reduced acoustic response as compared with monodisperse populations of microbubbles (Kaya et al. 2010; Phillips et al. 2010; Stride and Edirisinghe 2009; Talu et al. 2007)—prompting a shift towards monodisperse populations of microbubbles for ultrasound applications. While polydisperse microbubble populations can be sorted into subpopulations with narrower size distributions using various size sorting techniques (Feshitan et al. 2009; Huh et al. 2007; Kapishnikov et al. 2006; Kvale et al. 1996), these methods add complexity, rarely achieve a fine degree of monodispersity, and reduce overall yield. In contrast, microfluidic devices can produce monodisperse microbubbles with a polydispersity index of less than 5 % (Stride and Edirisinghe 2009).

Microfluidic devices direct gas and liquid phases through micrometer sized channels and apertures in order to use shear forces to produce microbubbles from a gas cone or jet. Several microfluidic device designs for microbubble production exist including: t-junction (Garstecki et al. 2006), v-junction (Gunduz et al. 2012b), co-flow (Gañán-Calvo and Gordillo 2001), coaxial electrohydrodynamic atomisation (CEHDA) (Farook et al. 2007), and flow-focusing microfluidic devices (FFMD) (Castro-Hernández et al. 2011; Cubaud et al. 2005; Garstecki et al. 2004; Gordillo et al. 2004; Hettiarachchi et al. 2007a; Talu et al. 2006). In addition, recent studies have used microfluidic devices to produce microbubbles in novel ways. Gunduz et al. (2012a) used a t-junction microfluidic device to produce particles that undergo further budding to produce microbubbles and Duncanson et al. (2012) produced droplets with a liquid/liquid center that chemically reacts to produce the gas core. While all these designs are capable of producing monodisperse distributions of microbubbles, FFMDs have found preference as they are produced by casting poly-dimethyl-siloxane (PDMS), a biocompatible synthetic polymer, onto molds fabricated using conventional microphotolithography (Duffy et al. 1998; McDonald et al. 2000). Photolithography allows intricate channel patterns to be produced at micrometer scales in a simple, low-cost, and time efficient fabrication process. FFMDs can be further categorized depending on the geometry of the outlet channel. In the expanding nozzle design, a velocity gradient develops as the gas and liquid phase pass through the narrow nozzle and into an expanding outlet (Tan et al. 2006). As a result, microbubble pinch-off occurs at lower flow rates, reducing waste. Furthermore, unlike agitation methods, the volume of the gas bubbles from an FFMD—for a given gas and liquid flow rate—is consistent after each pinch-off,

resulting in the production of a monodisperse population of microbubbles.

One factor that has limited adoption of microfluidic devices is low production rates (Stride and Edirisinghe 2009) of vascular compatible microbubbles (i.e.  $<10\ \mu\text{m}$ ). Current generation microbubbles such as DEFINITY<sup>®</sup> are dosed at approximately nine billion microbubbles for an average adult male with 98 % of the microbubbles less than  $10\ \mu\text{m}$  in diameter (Lantheus Medical 2008). These quantities and diameter are required to compensate for losses that occur during administration and circulation as a result of gas diffusion and filtration (Butler and Hills 1979; Iijima et al. 2006; Lim et al. 2004; Talu et al. 2008) and to reduce the risk of emboli (Goldberg et al. 1994). Production rates of stable lipid shelled microbubbles from an FFMD are on the order of  $10^3$  microbubbles per second (MB/s) (Hettiarachchi et al. 2009; Talu et al. 2006), with production rates decreasing to as little as 10 MB/s as microbubble diameters approach clinically useful (i.e.  $<10\ \mu\text{m}$ ) sizes (Kaya et al. 2010). While the microbubble production rate of an FFMD can be increased by manipulating flow rates, and fluid properties, this increase comes at the expense of reduced monodispersity (Hettiarachchi et al. 2007a). Production rates can also be increased by increasing the number of microbubble producing nozzles in a single FFMD (Barbier et al. 2006; Hashimoto et al. 2008; Hettiarachchi et al. 2007b; Li et al. 2008; Mulligan and Rothstein 2012), or by running several FFMDs simultaneously; however these parallelized devices can be difficult to operate. Equal pressures need to be supplied to each gas and liquid channel, which can require a complex 3D manifold (Love et al. 2001) in order to maintain monodispersity, and it is difficult to evenly distribute the pressure and flow conditions necessary to produce uniform, small, microbubbles ( $<10\ \mu\text{m}$ ) through all the channels. As a result, parallelized FFMD systems often produce microbubbles with large diameters ( $>100\ \mu\text{m}$ ), large size variation between nozzles, or are limited to producing liquid in liquid microdroplets.

In order to overcome these limitations, we propose the production of microbubbles in situ directly within the vasculature rather than production for storage. By producing microbubbles within the vasculature, loss due to injection and circulation is eliminated, thus significantly reducing the quantity of microbubbles necessary to provide sufficient contrast. As the microbubbles do not need to be stored, novel formulations can be investigated that include, for example, highly soluble but more biocompatible gases or lower stability shells. Most importantly, this relaxes the necessity for small (i.e.  $<10\ \mu\text{m}$ ) microbubble diameters.

Scattering efficiency of microbubbles has been shown to increase with the sixth power of diameter (Dalla Palma and Bertolotto 1999; Morse and Ingard 1968; Nishi 1972) and larger microbubbles have more surface area to carry a

potential therapeutic agent. Unfortunately, large microbubbles increase the risk of emboli. By combining unstable shells with biocompatible gases, larger microbubbles (i.e.  $>10\ \mu\text{m}$ ) can be produced that quickly dissolve if not destroyed by ultrasound, thus reducing emboli risk. Thus, in situ produced microbubbles can simultaneously exhibit the advantages of both large (increased ultrasound image contrast) and small microbubbles (superior safety). Alternatively, by varying the flow and pressure inlet conditions, microbubble diameter can be varied in real-time during a procedure according to preference (e.g. from an imaging mode using large microbubbles to a therapeutic mode using smaller microbubbles). Furthermore, an intravascular ultrasound catheter could be coupled to the in situ produced microbubbles allowing immediate visualization—and if necessary destruction. FFMDs are ideal for implementing in situ produced microbubbles as they can produce microbubbles in a continuous process in real-time while controlling the diameter. Unfortunately, in their current implementation FFMDs are difficult to miniaturize to the size necessary to fit within a vessel.

We have developed a new method for supplying the liquid phase to FFMDs that we believe will help reduce the footprint and enable miniaturization. Instead of supplying the liquid phase to all the inlets using a complex manifold, such as a 3D arrangement of discrete tubes or a maze of branching microfluidic channels, we have directly coupled the liquid inlets of the FFMD to a pressurized liquid compartment (Fig. 1a, b). This design provides three advances over current FFMD techniques. First, the number of tube-device interconnects are reduced as the liquid inlets can be directly plasma bonded to the liquid chamber. This allows the distance from the liquid inlets to the nozzle to be shortened as large inlets are not needed to accommodate the tubing interconnects. Furthermore, since a plasma bond is used, the connection is less likely to be clogged, as compared to epoxy bonds, or fail due to overpressure (Lo and Meng 2008). Second, this design simplifies FFMD parallelization. Additional liquid inlets for supplying additional nozzles can be introduced simply by drilling additional holes to link the interior flooded space to the necessary microfluidic liquid inlet. This significantly reduces the footprint of the device, as complicated mazes of branching microchannels are not needed, and helps to ensure equal liquid pressure gradients at all nozzles (Hettiarachchi et al. 2007b; Jiang et al. 2011). Finally, by simplifying production and reducing the footprint of FFMDs, the flooded design facilitates miniaturization. By eliminating large bulky interconnects and reducing the length of the microchannels, smaller FFMDs can be produced and, for example, be integrated into catheters intended for applications in the peripheral (2–5 mm in diameter) or coronary ( $\sim 1\ \text{mm}$  in diameter) vasculature.

In this paper, we present a novel method for producing and operating FFMDs. Using an optimal concentration of a shell material dispersed in the liquid phase, we characterize the relationship between liquid flow rate, gas pressure, microbubble diameter, and microbubble production rate. Both single nozzle and parallel nozzle FFMDs are characterized. Finally, we show proof-of-concept that in situ produced microbubbles can be imaged in real time using ultrasound.

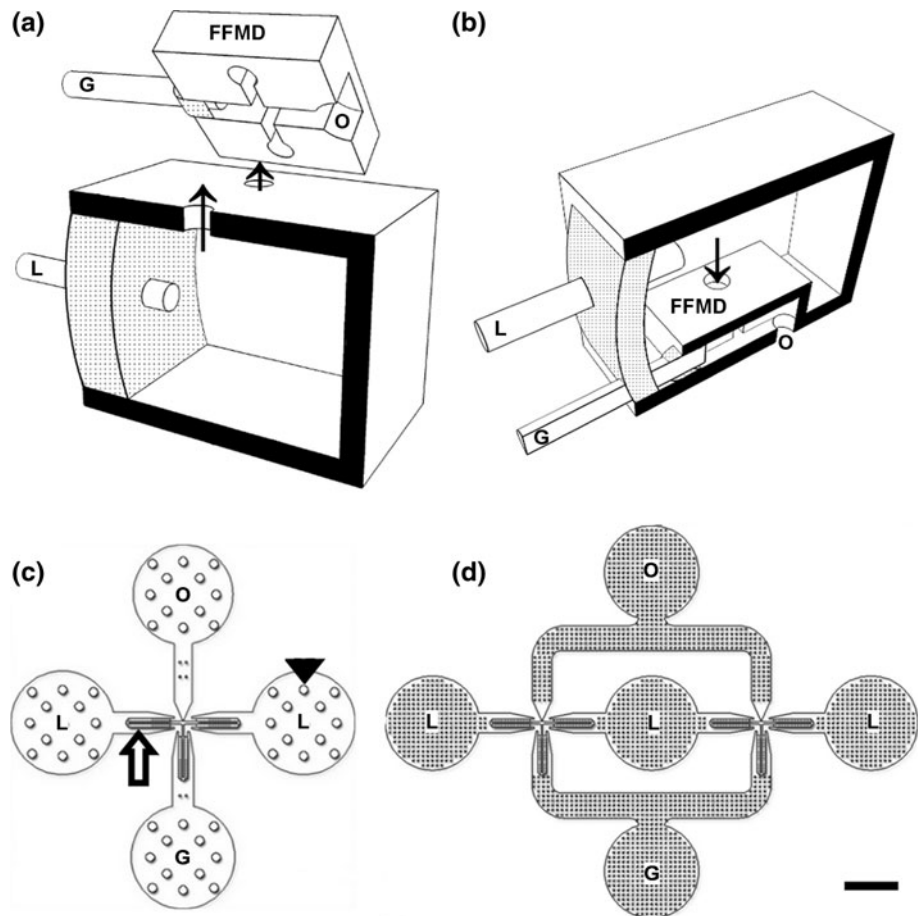
## 2 Materials and methods

### 2.1 Microfluidic device fabrication

Expanding nozzle flow-focusing microfluidic devices (FFMDs) were cast into poly-dimethyl-siloxane (PDMS) (Sylgard 184, Dow Corning, Midland, MI) using a custom fabricated mold (Duffy et al. 1998). The custom molds were fabricated by spinning a negative photoresist (SU8-3025, Microchem, Newton, MA) onto a silicon wafer then exposing the wafer to UV through a custom designed,  $0.1\ \mu\text{m}$  spot size quartz mask (Microtronics Inc, Newtown PA). Both single nozzle devices and parallelized two-nozzle devices were produced (Fig. 1c, d). All devices were designed to have the following features:  $5\ \mu\text{m}$  wide nozzle,  $5\ \mu\text{m}$  filters (arrow, Fig. 1) at all inlets to prevent clogging from PDMS debris (Hettiarachchi et al. 2007a), posts (arrowhead, Fig. 1) throughout the channels ( $36$  and  $160\ \mu\text{m}$  in diameter for the two-nozzle and single nozzle devices, respectively) to prevent channel collapse (Lee et al. 2008; Ryley and Pereira-Smith 2006),  $35\ \mu\text{m}$  wide gas channel,  $50\ \mu\text{m}$  wide liquid channels, and  $20\ \mu\text{m}$  height. The gas phase entered the device via the gas inlet (G) whereas the liquid phase entered from the liquid inlets (L) and intersected with the gas at the expanding nozzle to produce microbubbles. PDMS in a 10:1 prepolymer to curing agent ratio was poured onto the mold, degassed, and then cured at  $80\ ^\circ\text{C}$  for 30 min.

Two types of flooded FFMDs were produced: externally mounted flooded FFMDs (eFFMDs) and internally mounted flooded FFMDs (iFFMDs) (Fig. 1c, d). First, holes ( $0.65\ \text{mm}$ ) were drilled into a  $10\ \text{mm}$  square polystyrene cuvette (Fisher Scientific, Pittsburgh, PA) to create the liquid inlets ports for the eFFMDs or microbubble outlets ports for the iFFMDs. eFFMDs were then fabricated by plasma bonding (March II, Nordson March, Concord, CA) ( $60\ \text{W}$ ,  $1\ \text{min}$ ) a PDMS device to the outside of a pre-drilled cuvette treated for 20 min with a 1 % APTES solution (Vlachopoulou et al. 2009). Whereas iFFMDs were fabricated by first plasma bonding a thin layer of PDMS ( $25\ \text{W}$   $30\ \text{s}$ ) to the PDMS device before attaching the device to the interior of the cuvette with a two part epoxy

**Fig. 1** Schematics for **a** externally mounted (eFFMD) and **b** internally mounted (iFFMD) flooded flow-focusing microfluidic devices. (*G* gas inlet, *L* liquid inlet, *O* microbubble outlet, *FFMD* flow-focusing microfluidic device. *Black* indicates cut plane, *dotted* indicates epoxy. Not to scale). For both designs, gas is provided directly to the device via tubing while the liquid phase is pumped into a separate chamber, pressurizing the liquid, and ultimately forcing it through the ports connecting the chamber and the FFMD (*arrows*). Mask design for **c** single and **d** parallel nozzle flow-focusing microfluidic designs (*Scale* 1 mm). Common features between the two designs include: a single gas inlet, posts within the channels to prevent channel collapse (*arrow head*), and filters at the gas and liquid inlets to prevent debris from entering the flow-focusing nozzle (*open arrow*)



(Hysol RE2039 and HD3561, Henkel Corp. Mooresville, NC). A 0.76 mm inner diameter PTFE tube (Cole Parmer, Vernon Hills, IL) was then inserted into the gas inlet and sealed to the PDMS device with epoxy. Finally, a PTFE tube for supplying the liquid phase was placed inside the cuvette prior to sealing the chamber with epoxy and hot melt glue (McMaster-Carr Robbinsville, NJ). iFFMDs were also produced using a 3 mm square glass tube (S103, Vitrocom Mountain Lakes, NJ) and a 6 mm inner diameter glass pipette (Fisher Scientific, Pittsburgh, PA). Intravascular ultrasound (IVUS) coupled FFMDs were produced by placing a guiding tube down the center of the cuvette to allow an IVUS imaging catheter to be threaded through the device.

## 2.2 Optimization of microbubble shell

Microbubbles were stabilized using polyethylene-glycol-40-stearate (PEG40st) (Sigma-Aldrich, St. Louis, MO) as previously described (Hettiarachchi et al. 2007a; Talu et al. 2006). The liquid phase containing the shell material was produced by adding PEG40st to a solution of 10 % glycerol, 10 % propylene glycol, in Millipore purified deionized water (GPW). The solution was sonicated (XL2020,

Misonix, Farmingdale, NY) with a half-inch probe (40 % power, 30 min) to disperse micelles and large aggregates, and filtered through a 0.45  $\mu\text{m}$  syringe filter (Fisher Scientific, Pittsburgh, PA) prior to use to remove any additional aggregates. Microbubbles were generated using liquid phases containing decreasing concentrations of PEG40st until microbubble coalescence was observed at the FFMD nozzle. For microbubbles that did not coalesce at the nozzle, long-term stability was measured by collecting microbubbles onto a glass slide, acquiring time lapse brightfield images using an inverted microscope (IX71, Olympus, Center Valley, PA) and a video recorder (Vixia HF S21, Canon USA Inc. Lake Success, NY), and measuring microbubble diameter over time. Additionally, microbubble distributions were determined using a coulter counter (Coulter II, Beckman Coulter Brea, CA).

To determine biocompatibility, PEG40st solutions were incubated with confluent rat carotid smooth muscle cells for 5 min. The cells were then rinsed with phosphate buffered saline (PBS) and stained with propidium iodide (Sigma-Aldrich, St. Louis, MO), a marker of cell membrane permeability and a surrogate for cell death. The lowest PEG40st concentration that did not cause coalescence or cell permeability was considered optimal.

### 2.3 Microbubble production

The liquid phase consisted of PEG40st, at the optimal concentration as determined above, dispersed in a 10 % glycerol and 10 % propylene glycol solution (GPW). The gas phase consisted of 99.998 % pure nitrogen gas (GTS Welco, Richmond, VA). The liquid phase was supplied to the device using a syringe pump (PHD2000, Harvard Apparatus) at flow rates between 10 and 180  $\mu\text{L}/\text{min}$  while the gas phase was applied at pressures between 34.5 and 103 kPa. Pressure was set and maintained using a two-stage regulator (VTS 450D, Victor Technologies International, Inc., St. Louis, MO) and the pressure at the gas inlet was verified using a digital manometer (06-664-21 Fisher Scientific, Pittsburgh, PA).

Microbubbles were produced by first applying the liquid phase at the flow rate under investigation until the liquid pressurized chamber and all FFMD channels were completely flooded. The gas phase was then applied and maintained at the pressure under investigation. Images of microbubble production were captured using an inverted microscope connected to a high speed framing camera (SIMD24, Specialised Imaging, Simi Valley, CA) once a stable production stream was formed. Microbubble diameter and production rate were measured from the acquired images using ImageJ (v 1.46d NIH Bethesda, MD). The relationship between gas pressure, liquid flow rate, microbubble diameter, and production rate was investigated by incrementing the liquid flow rate in 2  $\mu\text{L}/\text{min}$  step sizes while maintaining a constant gas pressure. Microbubble diameter and production rate were then measured after each increment in flow rate. Measurements were repeated until the FFMD no longer stably produced monodisperse microbubbles. The gas pressure was then incremented, liquid flow rate reset, and the process repeated. Data was only collected for gas and liquid combinations that resulted in microbubbles less than 20  $\mu\text{m}$  in diameter (i.e. less than the height of the FFMD channels) to limit the effect of wall interaction on microbubble production dynamics.

### 2.4 Ultrasonic imaging

A gelatin phantom—6 % (W/V) gelatin (Type B, Fisher Scientific) and 1 % (W/V) Agar (Fisher Scientific) (Patil et al. 2009)—with a 1.79 cm diameter lumen was produced to simulate a vessel. Microbubble production rate and diameter size from the FFMD was verified optically prior to insertion into the phantom lumen. An oscillatory flow of deionized water was established through the lumen using a peristaltic pump (Unispense 340, Wheaton Industries, Millville, NJ). The manufactured microbubbles were imaged inside the vessel using a linear array connected to a

clinical ultrasound scanner (Siemens Sequoia 512 Scanner and 15L8 transducer, Siemens Medical Solutions, Malvern, PA). The microbubbles were imaged at a mechanical index (MI) of 0.2 and a center frequency of 14 or 7 MHz when using either fundamental B-Mode or a contrast agent specific nonlinear imaging mode (Contrast Pulse Sequences [CPS] Phillips 2001), respectively. Flow was stopped and the MI was set to 1.9 on the linear array while in CPS mode in order to investigate microbubble destruction. In situ manufactured microbubbles were also imaged with a coupled IVUS-FFMD using a 45 MHz intravascular ultrasound (IVUS) catheter connected to a clinical IVUS imaging system (InVision Gold Scanner and Revolution catheter, Volcano Corp. San Diego, CA).

## 3 Results and discussion

### 3.1 FFMD fabrication and shell material optimization

Both externally mounted flooded FFMDs (eFFMDs) and internally mounted flooded FFMDs (iFFMDs) were successfully fabricated. The final nozzle and filter widths were 8  $\mu\text{m}$ . All other dimensions were produced as designed. The simplification of construction allowed for a significant reduction in FFMD size. The smallest iFFMD manufactured to date measures  $14.5 \times 2.8 \times 2.3$  mm. While eFFMDs and iFFMDs share the same fundamental design—a common liquid pressurized chamber in order to apply a constant liquid pressure across all liquid inlets—each device has advantages and disadvantages. The iFFMD requires fewer drilled holes in the wall of the pressurized chamber. Alignment is easier as only the microbubble outlet port needs access to the outside. eFFMD, however, requires access to each liquid inlet so multiple holes need to be aligned to the ports. The most important difference is the pressure applied to the microfluidic device. In eFFMDs, the channels in the microfluidic device are not subject to the pressures inside the liquid chamber while in the iFFMD, the microfluidic device needs to withstand the pressure necessary to drive liquid through the inlets.

Initial testing of the FFMDs used the surfactant Tween 20 (Castro-Hernández et al. 2011; Garstecki et al. 2004; Gordillo et al. 2004) (Sigma-Aldrich, St. Louis, MO) in the liquid phase to stabilize the microbubble shell. We observed that concentrations above 2 mg/mL were required to produce stable microbubbles at a high production rate; however, concentrations of Tween 20 as low as 0.5 mg/mL are known to lyse cells (Sigma-Aldrich 2012). Phospholipids such as 1,2-distearoyl-sn-glycero-3-phosphocholine (DSPC) (Avanti Polar Lipids, Alabaster, AL) are also commonly used as a shell material to stabilize the microbubble (Hettiarachchi et al. 2007a; Kaya et al. 2010; Talu

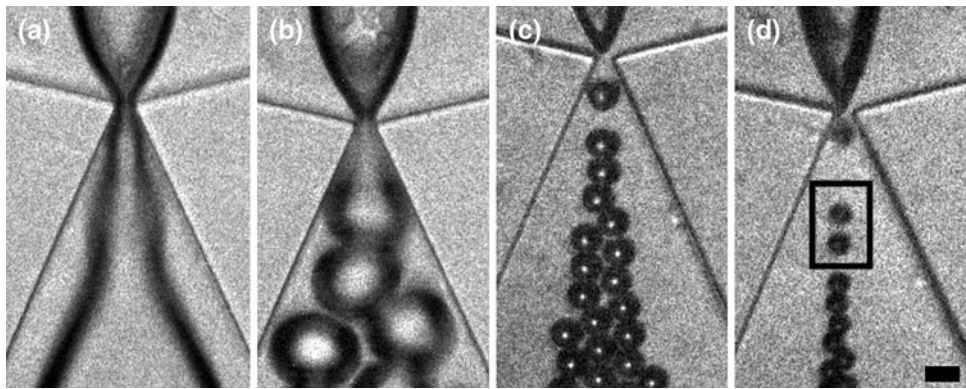


**Fig. 2** Microbubble production regimes of flooded FFMDs. Scale bar 10  $\mu\text{m}$  for all figures. **a** I: Overpressure ( $<34 \mu\text{L}/\text{min}$ ), the gas pressure overwhelms the liquid flow rate and no microbubbles are produced. **b** II: Cylindrical ( $34\text{--}60 \mu\text{L}/\text{min}$ ), microbubbles are larger than the height of the microfluidic channel resulting in the production of non-spherical microbubbles. **c** III: Stable ( $60\text{--}80 \mu\text{L}/\text{min}$ ), microbubbles with diameters less than the height of the channel but greater than the nozzle width are stably produced. **d** IV: Unstable ( $80\text{--}92 \mu\text{L}/\text{min}$ ), microbubble production becomes unstable and can

result in doublet formation (i.e. two microbubbles in quick succession followed by a delay in microbubble production, *black box*) and microbubbles with diameters less than the nozzle width. **V**: Underpressure ( $>92 \mu\text{L}/\text{min}$ ), liquid flow overwhelms the gas pressure and no microbubbles are produced (not shown). Flow rates are representative for a gas pressure of 55.2 kPa. The flow rate range for each regime, however, changes with gas pressure, with regime III broadening with increasing gas pressure

et al. 2006) and were investigated. Solutions containing 2 mg/mL DSPC and 2 mg/mL PEG40st resulted in microbubble coalescence when production rates were increased above 90,000 microbubbles/s (MB/s) or when producing microbubbles smaller than 20  $\mu\text{m}$  in diameter. Increasing the concentration of DSPC to 20 mg/mL eliminated coalescence and allowed microbubbles as small as 12  $\mu\text{m}$  to be produced. However, at this concentration, production rates peaked at 3,900 MB/s—which we attribute to the increased liquid phase viscosity. Consequently, in order to obtain the high production rates of Tween 20 and the biocompatibility of lipid, PEG40st in a glycerol propylene glycol solution (Hettiarachchi et al. 2007a; Talu et al. 2006) was selected as the shell material. The optimal PEG40st concentration was determined to be 3 mg/mL. Microbubbles produced with PEG40st solutions at concentrations below 2.5 mg/mL coalesced immediately upon formation. Cells incubated with concentrations of PEG40st below 2 mg/mL exhibited no membrane permeabilization, while cells incubated with concentrations of PEG40st above 3 mg/mL exhibited complete membrane permeabilization. Although PEG40st at concentrations of 3 mg/mL caused cell permeabilization, only small volumes ( $<200 \mu\text{L}/\text{min}$ ) of the liquid phase will be exiting the microfluidic device during production. As a result, the PEG40st will quickly be diluted to concentrations that do not cause permeabilization. PEG40st stabilized microfluidic microbubbles were not as stable as microfluidic microbubbles stabilized with lipid (Hettiarachchi et al. 2007a; Talu et al. 2006), and exhibited a loss of polydispersity within 60 s after production. Our goal, however, is to utilize the unstable microbubbles in order to allow

microbubbles not destroyed immediately after production, whether for imaging or drug delivery, to dissolve.

### 3.2 Microbubble production and characterization

Both iFFMD and eFFMD were capable of producing monodisperse microbubbles. Microbubble production could be divided into five distinct regimes (Guillot and Colin 2005; Xu et al. 2006) (Fig. 2), with the boundaries between the regimes determined by the transition of production from one type of microbubble to another. The flow rate limits that defined each of these regimes depended on gas pressure. Overall, increases in the gas pressure increased the minimum flow rate at which a regime began as well as broadened the range of flow rates over which a regime occurred. Microbubble production was most stable when the produced microbubbles had diameters less than the height of the channel but greater than the nozzle width, which we term the stable regime. In addition, maximum production rate always occurred within the stable regime. As a result, flooded FFMDs were only operated and characterized in this regime. While it was possible to produce microbubbles with diameters that were smaller than the width of the nozzle, microbubble production would become unstable, production rate dropped precipitously, and microbubble multiplets (i.e. one or more microbubbles of different diameters produced in quick succession followed by a delay in microbubble production) began to form. Microbubbles with diameters larger than the height of the channel were not characterized in order to limit the effect of the wall on microbubble production dynamics.

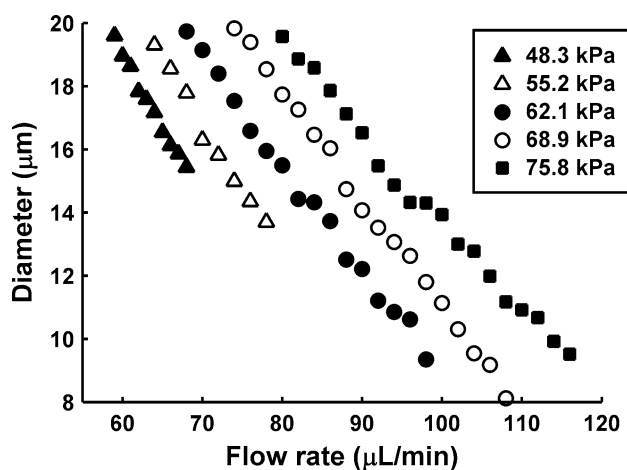


**Fig. 3** Diameter of eFFMD produced microbubbles as a function of liquid flow rate and gas pressure. Diameters were measured optically and are an average of independent runs ( $n = 3$ ). 95 % of the produced microbubbles had a polydispersity index less than 5 % and no microbubbles had a polydispersity index greater than 8 %. The liquid flow rate range capable of producing microbubbles increased and shifted rightward with increasing gas pressures. Increasing gas pressure also allowed progressively smaller microbubbles, approaching the nozzle width (8  $\mu\text{m}$ ), to be produced. Diameter as a function of flow rate was found to fit a linear trend with  $R^2 > 0.98$  for all pressures

While eFFMDs were capable of stably producing microbubbles at high production rates, iFFMDs were only able to produce microbubbles for short periods of time (approximately 10 min) during which microbubble diameter would decrease until production ceased—despite liquid flow rate and gas pressure remaining constant. However, if the liquid flow rate remained constant, progressively increasing gas pressure over time rescued microbubble production. One possible cause for the observed behavior was that the increasing pressure inside the liquid chamber compressed the compliant PDMS gas channel. This would cause gas flow rate to decrease, resulting in smaller microbubbles, until flow ceases altogether, and is consistent with our observations. The eFFMD design mitigates the problem by placing the FFMD outside the pressurized liquid chamber and thus preventing the collapse of the gas channel.

eFFMDs were characterized at gas pressures between 48 and 75 kPa. The minimum flow rate and the range of flow rates in which the eFFMD stably produced microbubbles smaller than the channel height increased as gas pressure increased. The minimum flow rate increased by 21  $\mu\text{L}/\text{min}$  and the range over which the eFFMD operated increased by 27  $\mu\text{L}/\text{min}$  between the lowest and highest gas pressures. For a given gas pressure, microbubble diameter decreased linearly with increasing liquid flow rate ( $R^2 > 0.98$  for all pressures) (Fig. 3), with the smallest microbubble produced just prior to transition out of the

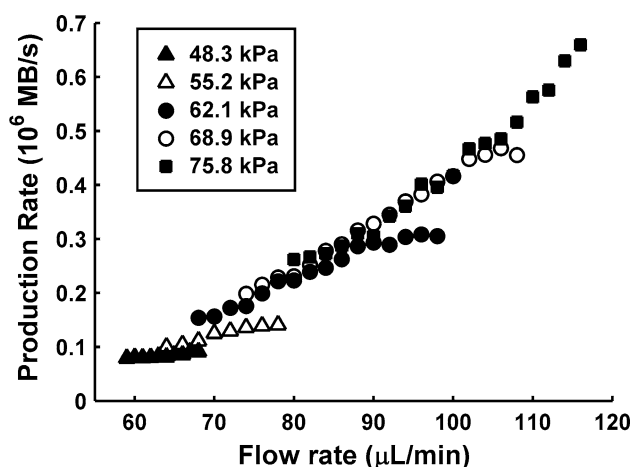


**Fig. 4** Production rate of eFFMD produced microbubbles as a function of liquid flow rate and gas pressure. Production rates were measured optically using a high speed camera and are an average of independent runs ( $n = 3$ ). 90 % of the production rates had a coefficient of variation less than 10 % and no production rate had a coefficient of variation greater than 21 %. Production rates increased linearly with flow rate ( $R^2 > 0.85$  for all pressures). Increasing gas pressure shifted production rate curves upward allowing for higher production rates. A maximum of 660,000 microbubbles per second (MB/s) was achieved

stable regime. In addition, the microbubble diameter became less sensitive to changes in liquid flow rate with increasing pressure. The smallest microbubble capable of being produced at a given pressure decreased for increasing pressures, with a plateau as the microbubble diameter approached the nozzle width. Production rate at a given gas pressure increased linearly (Fig. 4) with increasing liquid flow rate ( $R^2 = 0.85$  for 48.3 kPa and  $>0.95$  for all other pressures), peaking just prior to the transition out of the stable regime. In addition, production rate became more sensitive to changes in liquid flow rate with increasing pressure. The maximum production rate for a given pressure also increased with increasing pressure. These trends suggest that operating eFFMDs at higher gas pressures is optimal as it results in smaller microbubbles, higher production rates, and a wider range of liquid flow rates at which the device can operate stably. The last property provides improved control over microbubble diameter by increasing the separation between the liquid flow rates necessary to produce a microbubble of a specific size. Overall, the diameter of the smallest microbubble produced was 8.1  $\mu\text{m}$  and the maximum production rate was 660,000 microbubbles per second (MB/s) (Table 1).

In addition to increasing gas pressure, parallelized FFMDs were investigated as an alternative method for increasing microbubble production rate. A two nozzle parallelized eFFMD was successfully fabricated and characterized at 74.5 kPa (Fig. 5a). The microbubble diameter from the two nozzles were approximately equivalent with a

**Table 1** Microbubble production capabilities for single nozzle iFFMD and eFFMD, and a parallelized two-nozzle eFFMD

	iFFMD	eFFMD	Parallel eFFMD
Smallest diameter ( $\mu\text{m}$ )	$9.8 \pm 0.5$	$8.1 \pm 0.3$	$9.4 \pm 0.2$
Production rate @ smallest diameter (MB/s)	3,600	450,000	590,000
Flow rate ( $\mu\text{L}/\text{min}$ )	10	108	184
Gas pressure (kPa)	34.5	68.9	74.5
Max production rate (MB/s)	4,600	660,000	670,000
Diameter @ max production ( $\mu\text{m}$ )	$16.5 \pm 0.8$	$9.5 \pm 0.6$	$11.2 \pm 0.2$
Flow rate ( $\mu\text{L}/\text{min}$ )	10	116	168
Gas pressure (kPa)	41.4	75.8	74.5

Liquid phase was 3 mg/mL PEG40St in GPW solution. Gas phase was nitrogen. Diameter and production rate were determined optically. Production rate for the parallel device is the combined rate from each nozzle

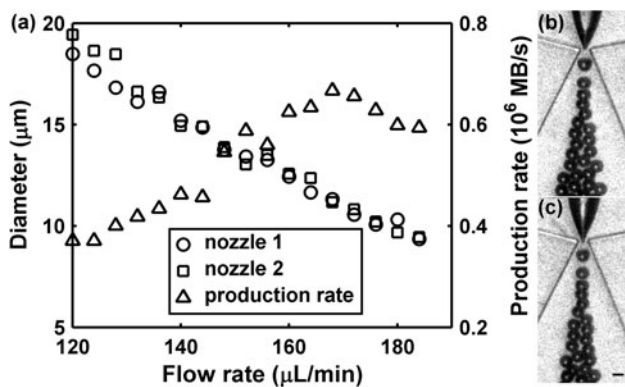


**Fig. 5** **a** Microbubble diameter and production rate for a two nozzle parallelized eFFMD at 74.5 kPa. Liquid phase was 3 mg/mL PEG40St in GPW solution. Gas phase was nitrogen. Polydispersity index was less than 4 % for all microbubbles. The combined data showed a linear trend between liquid flow rate and microbubble diameter ( $R^2 = 0.96$ ). Production rate is the combined number of microbubbles produced from both nozzles and a maximum of 670,000 microbubbles per second (MB/s) was achieved. **b**, **c** High speed camera images of the parallelized eFFMD, showing equivalent microbubble diameters and production rates from both nozzles. Scale bar 10  $\mu\text{m}$  for both images

mean difference in microbubble diameter between the two nozzles of 0.4  $\mu\text{m}$  (Fig. 5b, c). The smallest diameter microbubble produced by the parallelized eFFMD was  $9.4 \pm 0.2 \mu\text{m}$  at a production rate of 590,000 MB/s. The maximum combined production rate was 670,000 MB/s (Table 1). The polydispersity index was less than 4 % for all conditions in the parallel eFFMD. The maximum production rate of the parallelized device was equivalent to the maximum production rate achieved by a single nozzle eFFMD operating at 74.5 kPa. The parallelized eFFMD also exhibited a linear relationship between microbubble

diameter, production rate and liquid similar to those observed with a single nozzle eFFMD operating at the same pressure. However, unlike the single nozzle eFFMD, the production rate of the parallel eFFMD exhibits a peak followed by a drop before stable production ceases.

The discrepancy in maximum production may be due to the fluid dynamics of the parallel system. While each nozzle received the same gas pressures, it only received half the flow rate due to the parallel design. Therefore, the parallel eFFMD was equivalent to operating two single nozzle eFFMD at half the input liquid flow rates, resulting in the production of microbubbles from each nozzle at half the expected rate. Attempts to double the flow rate in order to compensate caused microbubble production to cease altogether. In addition, the design of our parallel device was slightly different than our single nozzle device. The parallel device had an increased density of support posts—increases fluid resistance of the channel—and a shared liquid inlet (Fig. 1b), rather than two independent inlets per nozzle (Fig. 1a). Together, these changes may have limited the production rate of the parallel device. As a control, two single FFMDs were bonded to the pressurized chamber to produce a pseudo-parallel eFFMD. When operated in this configuration, the pseudo-parallel eFFMD was capable of producing microbubbles at a rate 1.5 times greater than a single device operated under the same conditions, suggesting that a redesign of the parallel device may be necessary to realize increased production rates over single nozzle eFFMDs.

### 3.3 In situ microbubble imaging

Microbubbles produced in situ by an eFFMD were successfully imaged in real time using a 128 element linear ultrasonic imaging array (Siemens 15L8) at 14 MHz in B-mode and 7 MHz in CPS mode (Fig. 6). The microbubbles were produced at a rate of 222,000 MB/s, with a diameter of 14  $\mu\text{m}$ , and were acoustically active along the entire 13 cm length of the vessel. The microbubble filled lumen displayed a 23 dB increase in acoustic response over a water filled lumen and a 15 dB increase in acoustic response over the top wall (Fig. 6a, b). The eFFMD produced microbubbles also exhibited a strong acoustic response when imaged in CPS mode and all microbubbles within the transducer field of view were destroyed 30 s after increasing the MI to 1.9 (Fig. 6c, d). When imaged at 45 MHz using an IVUS catheter and imaging system, the microbubble filled lumen displayed a 15 dB increase over the water filled lumen even though the imaging frequency was approximately two orders of magnitude larger than the expected resonant frequency.

To date, microfluidic devices for microbubble production have been designed to produce stable microbubbles that



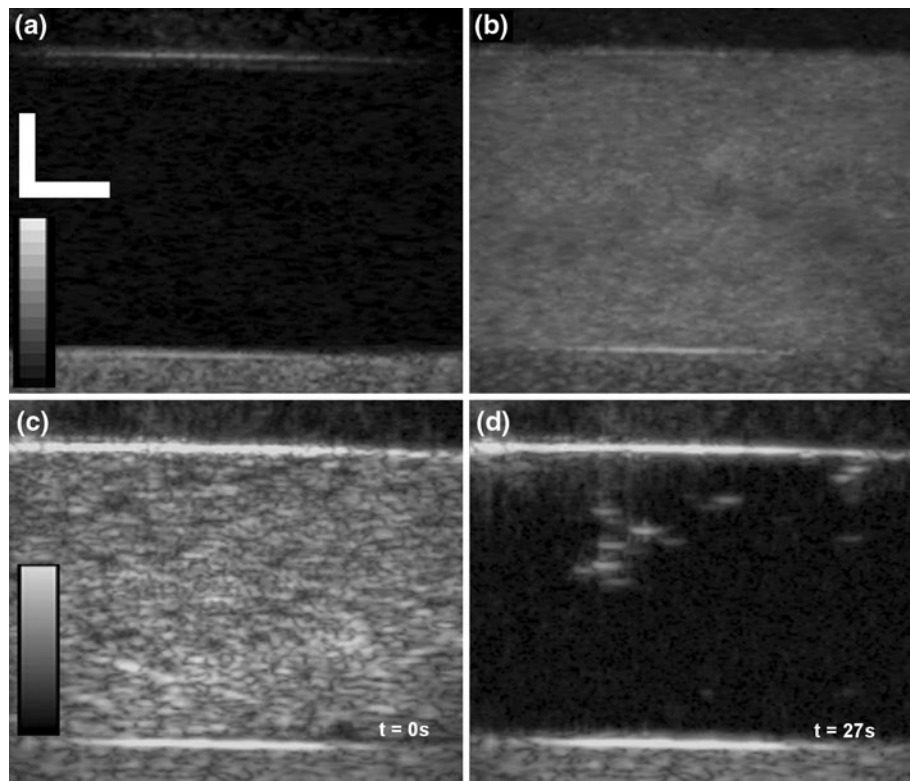


**Fig. 6** Ultrasound images of PEG40St microbubbles produced in situ via an eFFMD and imaged in real time with a 128 element linear array. **a** B-mode image ( $f_c = 14$  MHz,  $MI = 0.2$ ) of the 1.79 cm inner diameter lumen within the gelatin phantom before microbubble production. *Top row* dynamic range scale = 100 dB and gain = 0 dB. **b** B-mode image of 14  $\mu$ m diameter microbubbles produced at a rate of 222,000 MB/s. Microbubbles were under an 8 cm/s

peristaltic flow. **c** Contrast pulse sequence (CPS) mode ( $f_c = 7$  MHz) image of the microbubbles. *Bottom row* dynamic range scale = 100 dB and gain = 20 dB. Flow was temporarily stopped and the MI was increased to 1.9 in order investigate microbubble destruction. Complete destruction of all the microbubbles within the transducer field of view was observed after 30 s of insonation (**d**). *Scale bar* 5 mm in both directions and applies to all images

can be stored and utilized in the future, similar to the way approved formulations of microbubbles are used (Lantheus Medical 2008). To the best of the authors' knowledge, this report is the first description of microfluidic devices for the production of microbubbles intended for immediate use. Our flooded design enhances this capability by providing a means to reduce the dimensions of the microfluidic device to fit within the lumen of human vessels. Previous methods for producing microbubbles from microfluidic devices required viscous solutions of lipids and slow production rates to produce monodisperse microbubbles that could survive days to months (Talu et al. 2006). By producing microbubbles in situ and imaging them immediately, however, we can use a shell formulation that is less stable but allows for much higher microbubble production rates. While these rates may not be as high as those achieved by agitation methods, rates of 200,000 MB/s were more than adequate to provide significant and sufficient vessel contrast, as observed in the ultrasound images.

Catheter-based FFMDs are one application that could benefit from the advantages of the flooded FFMD design.

Catheter-based FFMDs hold promise for in situ production of microbubbles within the vessel of interest, allowing for the production, imaging, and destruction of microbubbles within the immediate vicinity of a therapeutic site. In situ production also significantly reduces the need for requiring microbubble stability/longevity. Microbubbles produced directly within vessels would only need to survive a few seconds, and over a few millimeters of transport to provide useful contrast or therapeutic effect (e.g. drug delivery). Consequently, unconventional microbubble designs, such as high solubility gas cores or unstable shell compositions, become feasible and possibly advantageous. For example, fluorocarbon gas may be replaced with oxygen, and gas dissolution (Kabalnov et al. 1998; Meltzer et al. 1980) away from the target can be relied upon to prevent the formation of a distant gas emboli. As a result, the production of larger ( $>10$   $\mu$ m) microbubbles, with increased scattering cross section and larger drug payload, may be envisaged without compromising safety. The flooded FFMD design would also help eliminate bulky interconnects and simplify parallelization allowing the catheter to

be smaller while producing an increased number of microbubbles—both of which are necessary for a successful catheter-based microbubble delivery system.

#### 4 Conclusions

We have successfully demonstrated the fabrication and operation of a new method for supplying the liquid phase to a flow-focusing microfluidic device (FFMD). By coupling the device to a chamber containing a pressurized liquid phase, complex manifolds and unnecessary tubing interconnects were eliminated. Flooded FFMDs were shown to produce microbubbles as small as 8  $\mu\text{m}$  and at production rates as high as 670,000 microbubbles per second. These sizes and production rates were shown to produce excellent ultrasound contrast when produced in situ and immediately imaged. In summary, this design simplifies FFMD parallelization and miniaturization and contributes towards our long-term goal of developing a therapeutic intravascular ultrasound catheter capable of in situ microbubble production, imaging, and drug delivery.

**Acknowledgments** This work was supported by the National Institutes of Health R01 HL90700. The authors would like to thank Dr. Arthur Weston Lichtenberger for his advice on photolithography, Dr. Alexander Klibanov for his advice on shell properties, and Dr. Paul Dayton for his help with the high speed camera. Volcano Corp provided a loan of equipment and IVUS catheters.

#### References

- Barbier V, Willaime H, Tabeling P, Jousse F (2006) Producing droplets in parallel microfluidic systems. *Phys Rev E* 74:046306. doi:10.1103/PhysRevE.74.046306
- Böhmer MR, Klibanov AL, Tiemann K et al (2009) Ultrasound triggered image-guided drug delivery. *Eur J Radiol* 70:242–253. doi:10.1016/j.ejrad.2009.01.051
- Butler BD, Hills BA (1979) The lung as a filter for microbubbles. *J Appl Physiol* 47:537–543
- Castro-Hernández E, van Hove W, Lohse D, Gordillo JM (2011) Microbubble generation in a co-flow device operated in a new regime. *Lab Chip* 11:2023–2029. doi:10.1039/c0lc00731e
- Chahal NS, Senior R (2010) Clinical Applications of Left Ventricular Opacification. *J Am Coll Cardiol Img* 3:188–196. doi:10.1016/j.jcmg.2009.09.022
- Cubaud T, Tatineni M, Zhong X, Ho C-M (2005) Bubble dispenser in microfluidic devices. *Phys Rev E Stat Nonlin Soft Matter Phys* 72:037302
- Dalla Palma L, Bertolotto M (1999) Introduction to ultrasound contrast agents: physics overview. *Eur Radiol* 9(Suppl 3):S338–S342
- Dayton PA, Rychak JJ (2007) Molecular ultrasound imaging using microbubble contrast agents. *Front Biosci* 12:5124–5142
- Duffy DC, McDonald JC, Schueller OJ, Whitesides GM (1998) Rapid prototyping of microfluidic systems in poly(dimethylsiloxane). *Anal Chem* 70:4974–4984. doi:10.1021/ac980656z
- Duncanson WJ, Abbaspourrad A, Shum HC et al (2012) Monodisperse gas-filled microparticles from reactions in double emulsions. *Langmuir* 28:6742–6745. doi:10.1021/la300915p
- Farook U, Zhang HB, Edirisinghe MJ et al (2007) Preparation of microbubble suspensions by co-axial electrohydrodynamic atomization. *Med Eng Phys* 29:749–754. doi:10.1016/j.medengphy.2006.08.009
- Farook U, Stride E, Edirisinghe MJ (2009) Preparation of suspensions of phospholipid-coated microbubbles by coaxial electrohydrodynamic atomization. *J R Soc Interface* 6:271–277. doi:10.1098/rsif.2008.0225
- Ferrara K, Pollard R, Borden M (2007) Ultrasound microbubble contrast agents: fundamentals and application to gene and drug delivery. *Annu Rev Biomed Eng* 9:415–447. doi:10.1146/annurev.bioeng.8.061505.095852
- Feshitan JA, Chen CC, Kwan JJ, Borden MA (2009) Microbubble size isolation by differential centrifugation. *J Colloid Interface Sci* 329:316–324. doi:10.1016/j.jcis.2008.09.066
- Fritz TA, Unger EC, Sutherland G, Sahn D (1997) Phase I clinical trials of MRX-115. A new ultrasound contrast agent. *Invest Radiol* 32:735–740
- Gañán-Calvo AM, Gordillo JM (2001) Perfectly monodisperse microbubbling by capillary flow focusing. *Phys Rev Lett* 87:274501
- Garstecki P, Gitlin I, DiLuzio W et al (2004) Formation of monodisperse bubbles in a microfluidic flow-focusing device. *Appl Phys Lett* 85:2649–2651. doi:10.1063/1.1796526
- Garstecki P, Fuerstman MJ, Stone HA, Whitesides GM (2006) Formation of droplets and bubbles in a microfluidic T-junction—scaling and mechanism of break-up. *Lab Chip* 6:437–446. doi:10.1039/B510841A
- Gessner R, Dayton PA (2010) Advances in molecular imaging with ultrasound. *Mol Imaging* 9:117–127
- Goldberg BB, Liu JB, Forsberg F (1994) Ultrasound contrast agents: a review. *Ultrasound Med Biol* 20:319–333
- Gordillo JM, Cheng Z, Ganan-Calvo AM et al (2004) A new device for the generation of microbubbles. *Phys Fluids* 16:2828. doi:10.1063/1.1737739
- Guillot P, Colin A (2005) Stability of parallel flows in a microchannel after a T junction. *Phys Rev E* 72:066301. doi:10.1103/PhysRevE.72.066301
- Gunduz O, Ahmad Z, Stride E et al (2012a) Bioinspired bubble design for particle generation. *J R Soc Interface* 9:389–395. doi:10.1098/rsif.2011.0671
- Gunduz O, Ahrnad Z, Stride E, Edirisinghe M (2012b) A device for the fabrication of multifunctional particles from microbubble suspensions. *Mater Sci Eng C-Mater Biol Appl* 32:1005–1010. doi:10.1016/j.msec.2012.01.018
- Hashimoto M, Shevkoplyas SS, Zasońska B et al (2008) Formation of bubbles and droplets in parallel, coupled flow-focusing geometries. *Small* 4:1795–1805. doi:10.1002/sml.200800591
- Hettiarachchi K, Talu E, Longo ML et al (2007a) On-chip generation of microbubbles as a practical technology for manufacturing contrast agents for ultrasonic imaging. *Lab Chip* 7:463–468. doi:10.1039/b701481n
- Hettiarachchi K, Talu E, Longo ML et al (2007b) Multi-array flow-focusing devices to accelerate production of microbubbles for contrast-enhanced ultrasound imaging. In: Eleventh international conference on miniaturized systems for chemistry and life sciences. Paris, France, pp 664–666
- Hettiarachchi K, Zhang S, Feingold S et al (2009) Controllable microfluidic synthesis of multiphase drug-carrying lipospheres for site-targeted therapy. *Biotechnol Prog* 25:938–945. doi:10.1002/btpr.214
- Huh D, Bahng JH, Ling Y et al (2007) Gravity-driven microfluidic particle sorting device with hydrodynamic separation amplification. *Anal Chem* 79:1369–1376. doi:10.1021/ac061542n
- Iijima H, Moriyasu F, Miyahara T, Yanagisawa K (2006) Ultrasound contrast agent, Levovist microbubbles are phagocytosed by

- Kupffer cells-in vitro and in vivo studies. *Hepato Res* 35:235–237. doi:10.1016/j.hepres.2006.04.016
- Jiang C, Li X, Yan F et al (2011) Microfluidic-assisted formation of multifunctional monodisperse microbubbles for diagnostics and therapeutics. *Micro Nano Lett* 6:417–421. doi:10.1049/mnl.2011.0141
- Kabalnov A, Klein D, Pelura T et al (1998) Dissolution of multicomponent microbubbles in the bloodstream: 1. Theory. *Ultrasound Med Biol* 24:739–749
- Kapishnikov S, Kantsler V, Steinberg V (2006) Continuous particle size separation and size sorting using ultrasound in a micro-channel. *J Stat Mech* 2006:P01012–P01012. doi:10.1088/1742-5468/2006/01/P01012
- Kaya M, Feingold S, Hettiarachchi K et al (2010) Acoustic responses of monodisperse lipid-encapsulated microbubble contrast agents produced by flow focusing. *Bubble Sci Eng Technol* 2:33–40
- Keller MW, Feinstein SB, Watson DD (1987) Successful left ventricular opacification following peripheral venous injection of sonicated contrast agent: an experimental evaluation. *Am Heart J* 114:570–575. doi:10.1016/0002-8703(87)90754-X
- Klibanov A (2002) Ultrasound contrast agents: development of the field and current status. In: Krause W (ed) *Contrast agents II*. Springer, Berlin, pp 73–106
- Kvale S, Jakobsen HA, Asbjornsen OA, Omtveit T (1996) Size fractionation of gas-filled microspheres by flotation. *Sep Technol* 6:219–226. doi:10.1016/S0956-9618(96)00157-9
- Lantheus Medical (2008) Definity (Package Insert). Lantheus Medical Imaging, N. Billerica, MA
- Lee J-K, Kung MC, Kung HH, Mockros LF (2008) Microchannel technologies for artificial lungs: (3) open rectangular channels. *ASAIO J* 54:390–395. doi:10.1097/MAT.0b013e31817eda02
- Li W, Young EWK, Seo M et al (2008) Simultaneous generation of droplets with different dimensions in parallel integrated microfluidic droplet generators. *Soft Matter* 4:258–262. doi:10.1039/B712917C
- Lim AKP, Patel N, Eckersley RJ et al (2004) Evidence for spleen-specific uptake of a microbubble contrast agent: a quantitative study in healthy volunteers. *Radiology* 231:785–788. doi:10.1148/radiol.2313030544
- Lo R, Meng E (2008) Integrated and reusable in-plane microfluidic interconnects. *Sens Actuator B-Chem* 132:531–539. doi:10.1016/j.snb.2007.11.024
- Love JC, Anderson JR, Whitesides GM (2001) Fabrication of three-dimensional microfluidic systems by soft lithography. *MRS Bull* 26:523–528. doi:10.1557/mrs2001.124
- McDonald JC, Duffy DC, Anderson JR et al (2000) Fabrication of microfluidic systems in poly(dimethylsiloxane). *Electrophoresis* 21:27–40. doi:10.1002/(SICI)1522-2683(20000101)21:1<27:AID-ELPS27>3.0.CO;2-C
- Meloni MF, Livraghi T, Filice C et al (2006) Radiofrequency ablation of liver tumors: the role of microbubble ultrasound contrast agents. *Ultrasound Q* 22:41–47
- Meltzer RS, Tickner EG, Popp RL (1980) Why do the lungs clear ultrasonic contrast? *Ultrasound Med Biol* 6:263–269
- Morse PM, Ingard KU (1968) *Theoretical acoustics*. Princeton University Press, Princeton, NJ
- Mulligan MK, Rothstein JP (2012) Scale-up and control of droplet production in coupled microfluidic flow-focusing geometries. *Microfluid Nanofluid* 13:65–73. doi:10.1007/s10404-012-0941-7
- Mulvagh SL, DeMaria AN, Feinstein SB et al (2000) Contrast echocardiography: current and future applications. *J Am Soc Echocardiogr* 13:331–342
- Nishi RY (1972) Ultrasonic detection of bubbles with Doppler flow transducers. *Ultrasonics* 10:173–179
- Patil AV, Rychak JJ, Allen JS et al (2009) Dual frequency method for simultaneous translation and real-time imaging of ultrasound contrast agents within large blood vessels. *Ultrasound Med Biol* 35:2021–2030. doi:10.1016/j.ultrasmedbio.2009.07.003
- Phillips PJ (2001) Contrast pulse sequences (CPS): imaging nonlinear microbubbles. In: *IEEE ultrasonics symposium*, vol 2. Atlanta, GA, pp 1739–1745
- Phillips LC, Klibanov AL, Wamhoff BR, Hossack JA (2010) Ultrasound-microbubble-mediated drug delivery efficacy and cell viability depend on microbubble radius and ultrasound frequency. In: *IEEE*, pp 1775–1778
- Ryley J, Pereira-Smith OM (2006) Microfluidics device for single cell gene expression analysis in *Saccharomyces cerevisiae*. *Yeast* 23:1065–1073. doi:10.1002/yea.1412
- Sigma-Aldrich (2012) Tween 20 product information. Sigma-Aldrich, St. Louis, MO
- Stride E, Edirisinghe M (2009) Novel preparation techniques for controlling microbubble uniformity: a comparison. *Med Biol Eng Comput* 47:883–892. doi:10.1007/s11517-009-0490-8
- Talu E, Lozano MM, Powell RL et al (2006) Long-term stability by lipid coating monodisperse microbubbles formed by a flow-focusing device. *Langmuir* 22:9487–9490. doi:10.1021/la062095+
- Talu E, Hettiarachchi K, Zhao S et al (2007) Tailoring the size distribution of ultrasound contrast agents: possible method for improving sensitivity in molecular imaging. *Mol Imaging* 6:384–392
- Talu E, Powell RL, Longo ML, Dayton PA (2008) Needle size and injection rate impact microbubble contrast agent population. *Ultrasound Med Biol* 34:1182–1185. doi:10.1016/j.ultrasmedbio.2007.12.018
- Tan Y-C, Cristini V, Lee AP (2006) Monodispersed microfluidic droplet generation by shear focusing microfluidic device. *Sens Actuators B Chem* 114:350–356. doi:10.1016/j.snb.2005.06.008
- Vlachopoulou M-E, Tserepi A, Pavli P et al (2009) A low temperature surface modification assisted method for bonding plastic substrates. *J Micromech Microeng* 19:015007. doi:10.1088/0960-1317/19/1/015007
- Wei K, Jayaweera AR, Firoozan S et al (1998) Quantification of myocardial blood flow with ultrasound-induced destruction of microbubbles administered as a constant venous infusion. *Circulation* 97:473–483
- Xu JH, Li SW, Wang YJ, Luo GS (2006) Controllable gas-liquid phase flow patterns and monodisperse microbubbles in a microfluidic T-junction device. *Appl Phys Lett*. doi:10.1063/1.2189570